



This is a repository copy of *An Analytical Study of the Dynamics of Binary Distillation Columns*.

White Rose Research Online URL for this paper:
<http://eprints.whiterose.ac.uk/85731/>

Monograph:

Edwards, J.B. and Jassim, H.J. (1975) *An Analytical Study of the Dynamics of Binary Distillation Columns*. Research Report. ACSE Research Report 37 . Department of Automatic Control and Systems Engineering

Reuse

Unless indicated otherwise, fulltext items are protected by copyright with all rights reserved. The copyright exception in section 29 of the Copyright, Designs and Patents Act 1988 allows the making of a single copy solely for the purpose of non-commercial research or private study within the limits of fair dealing. The publisher or other rights-holder may allow further reproduction and re-use of this version - refer to the White Rose Research Online record for this item. Where records identify the publisher as the copyright holder, users can verify any specific terms of use on the publisher's website.

Takedown

If you consider content in White Rose Research Online to be in breach of UK law, please notify us by emailing eprints@whiterose.ac.uk including the URL of the record and the reason for the withdrawal request.



eprints@whiterose.ac.uk
<https://eprints.whiterose.ac.uk/>

University of Sheffield
Department of Control Engineering

An Analytical Study of the Dynamics of Binary
Distillation Columns

J. B. Edwards and H. J. Jassim

Research Report No. 37

October 1975

An Analytical Study of the Dynamics of Binary
Distillation Columns

J. B. Edwards* and H. J. Jassim*

Abstract Analytical transfer function matrices are developed for describing the dynamic behaviour of the compositions within the rectifying and stripping sections of both very short and very long distillation columns, in response to changes in energy and liquid throughput. Matrices of first-order lags are shown to describe both situations very closely and the simple structure of the models demonstrates the need to consider only steady-state operating curves for the elimination of interaction problems arising in twin product control.

The models are useable directly by the plant or design engineer who merely needs to substitute basic design data to obtain good estimates of all the model parameter values. An elementary inverse Nyquist approach is presented which predicts precisely the extent of the detuning of one composition control loop by closing the other loop.

The long column model is shown to have much in common with models produced by other authors who have used widely different, and usually partly-empirical, approaches to column modelling. The analytical approach here proves, for specified conditions, the empirical observations relied upon by these previous workers. The modelling method used here involves the solution of the process partial differential equation at high frequency and the discrete process equations at low frequency. The two resulting models join together quite naturally because of their structural similarity. It is believed that the approach could find application in separation processes generally.

* Department of Control Engineering, University of Sheffield, England.

1. Introduction

Process models expressed in the form of a matrix of transfer functions are valuable for predicting process behaviour in response to small disturbances and for assessing the performance of control systems. Their value to the practising engineer is increased enormously if the model parameters can be related to the basic design parameters of the plant and its pre-specified operating conditions. The analytical determination of such relationships has the advantage over an empirical approach in that the former provides a deeper insight into the process behaviour and generates fairly precise confidence limits on the range of conditions to which the model is applicable. Because of the need to idealise process equations, however, the analytic model predictions must be shown to agree with well-established empirical results before the idealising assumptions can themselves be validated.

The binary distillation process has so far proved to be far from amenable to the analytical approach although significant efforts by Wilkinson and Armstrong¹ in 1957 and Wood and Armstrong² in 1960 did produce transfer functions between the compositions of the products and that of the feed. Unfortunately feed composition is rarely available for manipulation by the control system and the dynamic affects of changes in, say, reflux flow rate, L , or vapour rate, V , although related, are very different, as will be demonstrated. Stainthorp and Searson³ have more recently developed simple models for the response to changes in V and L based on a partly-analytic, approach, validating their model predictions on two industrial columns. Their approach was partly empirical, however, in that a key step in solving the process equations involved the use of a dynamic interrelationship between consecutive tray compositions determined from pilot-plant observations. Shinskey's⁴ approach is again analytic apart from one key assumption, empirically justified, of a unique relationship between V and the column separation factor, S . Davison⁵ developed a detailed dynamic model completely analytically but left this in terms of partial derivatives having little immediate relation to basic plant parameters.

Of course a wealth of material has been published on the application of control system design techniques, both optimal⁶ and frequency response⁷ based, to models derived from tests on specific columns and the strategies emerging have been evaluated practically by pilot plant trials by, often,

different authors, with varying degrees of success. All this provides an invaluable library of experience the only problem with which is its immense size. Furthermore the main objective of a report has very often been the testing of an identification, or control design or computer technique rather than being specifically devoted to acquiring column insight.

The need still exists for an approach to modelling column dynamics which yields an insight comparable to that offered by the McCabe-Thiel method⁸ for steady-state design. At an international symposium in 1969, Professor H. H. Rosenbrock⁹ acting as rapporteur for a session on columns stated: "In particular, any results which increase understanding and insight into the dynamic behaviour, (of distillation columns), are doubly rewarding. They can often confirm that difficulties will not arise so that a detailed investigation need not be made. On the other hand, when they show that difficulties can arise they may also suggest ways in which these difficulties can be overcome, again without the need for a full investigation". The present paper is an attempt to meet this need and the results do give much of the insight called for. The study begins with an investigation of the simplest possible type of still comprising essentially only two theoretical plates, and then moves to the case of a semi-infinite column.

2. Small Column

By way of introduction we consider first an ideal single-tray rectifier of molar holdup H_r surmounting merely the reboiler of holdup H_s . The term "ideal" indicates here adiabatic conditions, negligible sensible heat changes, equal molar latent heats, constant molar liquid holdup and negligible vapour holdup and a boiling liquid feed i.e. the standard case generally used to introduce steady-state design concepts. The total condenser is assumed to have negligible capacitance. Under these conditions the mass-balance equations for the lighter component for the rectifier and reboiler are:

$$\begin{aligned} & V(Y'-Y) + L(Y-X) = H_r \dot{X} \\ \text{and} \quad & F(Z-X') - V(Y'-X') + L(X-X') = H_s \dot{X}' \end{aligned} \quad \left. \vphantom{\begin{aligned} & V(Y'-Y) + L(Y-X) = H_r \dot{X} \\ & F(Z-X') - V(Y'-X') + L(X-X') = H_s \dot{X}' \end{aligned}} \right\} \dots (1)$$

and these together with a vapour/liquid equilibrium relationship, (assumed to hold throughout), of the form, say:

$$\alpha = \frac{Y(1-X)}{X(1-Y)} = \frac{Y'(1-X')}{X'(1-Y')} = \text{constant relative volatility} \quad \dots(2)$$

provide a complete specification of the process, if variables V,L,F and Z are known and X,Y,X' and Y' are unknown.

2.1. Steady State Behaviour

Steady-state data is valuable for choosing reasonable operating conditions under which to study the process dynamically, and such data is easily digested if presented graphically. The Y v X' plane offers a useful basis for presentation, as, for instance, in the McCabe-Thiel approach. Now a steady-state mass-balance on the whole column gives the general result:

$$Y = (1-F/D)X' + FZ/D \quad \dots(3)$$

$$\text{where } D = V-L \quad \dots(4)$$

so that Y must be linearly related to X' for constant feed conditions, the line slope being determined by the D/F ratio only and the line passing always through the point Z,Z. Within this plane combinations of terminal compositions are restricted to lie within a domain bounded by minimum and maximum separation lines. Column separation, S, is by definition given by

$$S = \frac{Y(1-X')}{X'(1-Y)} \quad \dots(5)$$

and its maximum value, which is approached at very high vapour rates, is given by the Fenske formula:

$$S_{\max} = \alpha^{P+1} \quad \dots(6)$$

where P = number of actual trays. (The result is easily derived from the steady-state versions of equations 1, by setting $V \gg F$). Here $S_{\max} = \alpha^2$ and S_{\min} is obviously α , a situation pertaining to zero reflux, (or $D = V$), when the column acts as a simple still. The permissible crescent shaped area which can be practically occupied by points Y,X' is illustrated in figure 1 for the case of $\alpha = 8.0$.

As well as straight loci of constant D/F, curves of constant V/F can also be determined analytically via equations 1, although with greater difficulty. As would be expected, for very large values of V/F, these loci follow closely the form of the upper permissible boundary

and therefore are similar in shape to lines of constant separation as assumed throughout by Shinsky⁴. For more economical energy throughputs however their form changes significantly in the 1-tray column as the curves of figure 1 indicate. Their slope never-the-less remains positive. (Figure 2 shows the computed loci for a 4-tray column having the same maximum separation, (64), as the single tray process and demonstrates the increasing tendency towards a one-to-one correspondence between V/F and S as columns become longer). As will be actually proved, an approximate knowledge of the form and location of these loci for any binary column is really all that is ultimately required for resolving the problems of interaction between the composition control loops under normal circumstances. Loci of constant L/F or constant R can be immediately determined from those for constant V/F and D/F. The former are also presented in figures 1 and 2.

2.2. Dynamic Model

Linearising process equations 1 for small perturbations x', y, v and ℓ in X', Y, V and L respectively, and taking Laplace transforms with respect to time yields, after some algebraic manipulation, a matrix equation of the form

$$[\tilde{y}, \tilde{x}']^T = [G(s)] [\tilde{v}, \tilde{\ell}]^T \quad \dots (7)$$

where the transfer-function matrix, $G(s)$

$$= \begin{bmatrix} -\alpha_r \left\{ \frac{(Y'-X')V\alpha_s}{F+(\alpha_s-1)V+L} + (Y-Y')(1+T_s s) \right\}, & \alpha_r \left\{ \frac{(X-X')V\alpha_s}{F+(\alpha_s-1)V+L} + (Y-X)(1+T_s s) \right\} \\ - \left\{ \frac{(Y'-X')(1+T_r s) [(V-L)\alpha_r + L] + (Y-Y')L}{F+(\alpha_s-1)V+L} \right\}, & \left\{ \frac{(X-X')(1+T_r s) [(V-L)\alpha_r + L] + (Y-X)L}{F+(\alpha_s-1)V+L} \right\} \end{bmatrix}$$

$$\times \frac{F+(\alpha_s-1)V+L}{\{(V-L)\alpha_r + L\}(1+T_s s)(1+T_r s)\{F+(\alpha_s-1)V+L\} - LV\alpha_s} \quad \dots (8)$$

where $T_s = H_s / \{F+(\alpha_s-1)V+L\} \quad \dots (9), \quad T_r = H_r / \{(V-L)\alpha_r + L\} \quad \dots (10)$

and $\alpha_s = \partial Y' / \partial X' \quad \dots (11), \quad \alpha_r = \partial Y / \partial X \quad \dots (12)$

Choosing as an initial working point one which allows easily observable changes in both outputs, X' and Y, to be produced by input perturbations, either v or l, of reasonable size, yields the point Y, X' = 0.8, 0.2 (see figure 1). At this working point the quiescent operating conditions are: Y = 0.8, X = 0.333, X' = 0.2, Y' = 0.666, D/F = 0.5, V/F = 0.7, L/F = 0.2, W/F = 0.5, Z = 0.5, $\alpha_r = 0.72$ and $\alpha_s = 1.39$. Substituting these values in equation 8 gives the numerical result

$$G(s) = \begin{bmatrix} -\left\{ \frac{0.79+0.24T_s s}{(1+T_s s)(1+T_r s)-0.236} \right\} 0.72, & \left\{ \frac{0.992+0.835T_s s}{(1+T_s s)(1+T_r s)-0.236} \right\} 0.72 \\ -\left\{ \frac{0.3685+0.316T_r s}{(1+T_s s)(1+T_r s)-0.236} \right\}, & \left\{ \frac{0.2034+0.0904T_r s}{(1+T_s s)(1+T_r s)-0.236} \right\} \end{bmatrix} \dots(13)$$

Of course equation 7 is only one of many possible mathematical representations of the process dynamics, an alternative, in terms of inputs v and d, ($\equiv \Delta D$), being:

$$[\tilde{y}, \tilde{x}']^T = [Q(s)] [\tilde{v}, \tilde{d}]^T \dots(14)$$

where, for the particular case considered here,

$$Q(s) = \begin{bmatrix} \left\{ \frac{0.202+0.595T_s s}{(1+T_s s)(1+T_r s)-0.236} \right\} 0.72, & -\left\{ \frac{0.992+0.835T_s s}{(1+T_s s)(1+T_r s)-0.236} \right\} 0.72 \\ -\left\{ \frac{0.1651+0.2256T_r s}{(1+T_s s)(1+T_r s)-0.236} \right\}, & -\left\{ \frac{0.2034+0.0904T_r s}{(1+T_s s)(1+T_r s)-0.236} \right\} \end{bmatrix} \dots(15)$$

the steady-state gain terms of which may be checked by measurement of the slopes of the constant V and constant D' loci of figure 1.

2.3 Dynamic Behaviour

The inverse Nyquist loci of each of the constituent transfer functions $g_{11}, g_{12}, g_{21}, g_{22}$ and $q_{11}, q_{12}, q_{21}, q_{22}$ of the matrices G and Q are very well-behaved, exhibiting phase shifts $\neq 90^\circ$ and resembling a first order lag loci for all reasonable holdup-ratios, H_s/H_r , thus implying no difficulty in stabilising either the y-control loop, (loop-1), or the x'-control loop, (loop-2), irrespective of the choice of input variable: provided the other loop is left open. Due to interaction effects, however, the choice of

coupling is most important when the closed-loop control of both products is considered and the results of simulating the non-linear process with various couplings are summarised in table 1. In each case the P+I loops were tuned for good separate performance before testing their simultaneous behaviour with separate disturbances in each loop.

Table 1. Interaction effects with various input/output couplings			
Test Identification	Loop 1	Loop 2	Interaction effect
A	y to d	x' to v	Loop tuning virtually unaffected, transient interaction in both loops
B	y to v	x' to d	Loop tuning considerably worsened, transient interaction in both loops
C	y to l	x' to v	Loop tuning somewhat improved, some transient interaction in both loops
D	y to v	x' to l	Control lost completely

Figures 3 and 4 illustrate cases A and B respectively. A loop-1 reference-change from 0.75 to 0.85 is applied with the loop 2 reference set at 0.15 in figure 3 and 0.25 in figure 4. The controllers employed for figure 3 and 4 were, respectively:

$$\begin{bmatrix} y \\ x \end{bmatrix} = \begin{bmatrix} 0.0 & , & 1.0+4.17/T_r s \\ 1.0+1.79/T_r s & , & 0.0 \end{bmatrix} \begin{bmatrix} v \\ d \end{bmatrix} \quad \dots(16)$$

and

$$\begin{bmatrix} y \\ x \end{bmatrix} = \begin{bmatrix} 0.0+4.17/T_r s & , & 0.0 \\ 0.0 & , & 1.0+1.79/T_r s \end{bmatrix} \begin{bmatrix} v \\ d \end{bmatrix} \quad \dots(17)$$

The latter case (figure 4, equation 17) illustrates an attempt, by elimination of proportional action in loop-1, to produce complete instability through interaction and, as such, is a somewhat pessimistic rather than a typical result for case B. The production of significant oscillation in case B is a general observation never-the-less.

2.4. Prediction of Dynamic Behaviour by an Inverse Nyquist Approach

Most of the results of Section 2.3, *inter-alia*, are predictable, without resort to simulation, by means of a simple inverse Nyquist approach which was inspired by Shinskey and Bristol's "relative-gain matrix"⁴ method, but extended beyond the steady-state to cover the full frequency range. The method is based on the inverses, (reciprocals), of the constituent elements of a system-transfer function matrix H , (i.e. h_{11}^{-1} , h_{12}^{-1} , h_{21}^{-1} , h_{22}^{-1}) rather than on the elements h_{11}^* , h_{12}^* , h_{21}^* , h_{22}^* of the matrix inverse H^* , ($=H^{-1}$), as in Rosenbrock's inverse Nyquist array technique¹⁰.

If the open-loop system input and output vectors are $[\tilde{\theta}_{i1}, \tilde{\theta}_{i2}]^T$ and $[\tilde{\theta}_{o1}, \tilde{\theta}_{o2}]^T$ respectively then

$$\tilde{\theta}_{o1} = h_{11} \tilde{\theta}_{i1}, \quad \tilde{\theta}_{i2} = 0 \quad \dots (16)$$

$$\tilde{\theta}_{o1} = \left\{ h_{11} - \frac{h_{12} \cdot h_{21}}{h_{22}} \right\} \tilde{\theta}_{i1}, \quad \tilde{\theta}_{o2} = 0 \quad \dots (17)$$

and similar results apply to the three pairs of alternative input/output dependences. Equation 16 describes the loop 1 situation with θ_{o2} uncontrolled and equation 17, that with θ_{o2} controlled perfectly. The vectorial separation of the inverse Nyquist loci h_{11}^{-1} and $\{h_{11} - h_{12}/h_{22}\}^{-1}$ therefore give an immediate indication of the degree to which the tuning of loop 1 is affected by the ideal closure of loop 2. The inclusion of pre- and post-compensators and the cascading of control-loop dynamics in the loop under investigation is readily achieved.

Figure 5a and 5b show the inverse Nyquist plots pertaining to the control laws 16 and 17, (and figures 3 and 4) respectively. Figure 5a predicts immediately the already noted insensitivity of loop 1 tuning to loop 2 closure. It furthermore predicts the loop's resonant frequency, ω_r , ($\approx 1.4/T_r$) which correlates closely with the natural frequency ($\omega_n \approx 1.5/T_r$) as well as the 20-30% overshoot of the step response. For the coupling $y \rightarrow v$, $x' \rightarrow d$, figure 5b clearly shows the significant shift of the locus from outside the unit M -circle towards the critical point and predicts therefore the change from an overdamped to an oscillatory response on closure of loop 2. The predicted resonant frequency, ($\approx 2.5/T_r$), is higher than the natural frequency ($\approx 1.1/T_r$) obtained from simulation but, as figure 4 shows, this is clearly due to the limiting effect of the process non-linearities and linear simulation yields good frequency correlation.

The complete loss of control observed in case D, ($y \rightarrow v$, $x' \rightarrow \infty$), is obvious by application of the simple inverse Nyquist technique to the steady-state situation. We note from the relevant process equation, (13), that

$$G(o) = 1.31 \begin{bmatrix} -0.569 & , & 0.714 \\ -0.3685 & , & 0.2034 \end{bmatrix}$$

and hence, whereas $g_{11}(o) = -0.745$, $\{g_{11}(o) - g_{12}(o) \cdot g_{21}(o) / g_{22}(o)\} = +0.949$ indicating a complete reversal in loop-1 gain upon closure of loop-2.

The result is a general one since, as figures 1 and 2 illustrate, $\partial Y / \partial V|_L$, $|=g_{11}(o)|$, is always negative whilst $\partial Y / \partial V|_{X'}$, $|=g_{11}(o) + g_{12}(o) \cdot g_{21}(o) / g_{22}(o)|$, is always positive because the constant V/F loci must have a greater slope than the constant L/F loci.

The simple method used here does not however give a clear picture of the transient interaction persisting between loops. It merely predicts the effect of interaction on loop tuning and the change in the degree of loop stability so caused. Clearly it is essential that tuning one loop should not significantly de-tune another, and the present method predicts the extent of the tuning alteration exactly. If the extent of transient interaction is to be determined then Rosenbrock's technique¹⁰ must be applied requiring access to the U.M.I.S.T., C.A.D. package. Figures 6 and 7 show elements of the inverse Nyquist array, so computed, together with the band of Ostrowski circles, (which are computed from a knowledge of both* controllers), within which the final locus lies. There is no obvious prediction of tuning insensitivity in figure 6 which, in this respect at least, is therefore highly pessimistic, and the proposed method is preferable for making such predictions.

Finally it is noted that for this short column, for a very wide range of H_s / H_r , transient interaction can be virtually eliminated over the entire frequency range of interest merely by cascading a non-dynamic pre-compensator of the form

$$K = G^{-1}(o) \quad \dots(18)$$

with the process $G(s)$, (equation 13), thus making

$$h_{12}(o)h_{21}(o)/h_{22}(o) = 0 \quad \dots(19)$$

The two inverse Nyquist loci of the proposed method are now practically indistinguishable and the Ostrowski bands shrink enormously also, as shown in figure 8. Dynamic interaction is therefore eliminated by steady-state compensation.

* The method here proposed requires knowledge of only the loop under test for the construction of both loci. The inverse Nyquist array method can also predict a band (the Gershgorin band), enclosing the final locus, requiring data from the one loop but this band is far wider than the Ostrowski band.

3. Very Long Columns

The analytic determination of a transfer functions matrix for columns having several trays by manipulation of the highly interconnected mass-balance equations would be extremely tedious and the resulting formulae, if obtained, would be too complicated to yield the desired insight into the structure of such processes. As the number of plates increases however the composition profile through each of the two column sections tends towards a continuous function in space thus allowing the use of two partial differential equations, (p.d.e's), for the process description yielding a tractable solution. We shall show that the semi-infinite column's dynamic structure closely resembles that of the short column just analysed so permitting the assumption of a common dynamic structure for all columns within limits to be determined.

3.1 Steady-State Analysis

Such an analysis is required to provide the quiescent operating conditions appearing as constant parameters in the small-perturbation dynamic model derived in Section 3.2. Considering the n th tray of the N -plate rectifier, (numbering upwards), the mass balance for the lighter component is

$$VY(n-1) - VY(n) + LX(n+1) - LX(n) = 0 \quad \dots(20)$$

and the equilibrium relationship is simplified to the linear form:

$$Y(n) = \alpha_r X(n) + (1-\alpha_r) \quad \dots(21)$$

where α_r for a long column will be only marginally less than unity because of the low relative volatility of the mixture requiring many stages for its separation. Applying Taylor's theorem and truncating to the second derivative we obtain the differential equation:

$$k_r dX(n)/dn = d^2X(n)/dn^2 \quad \dots(22)$$

where $k_r = 2(V\alpha_r - L)/(V\alpha_r + L) \quad \dots(23)$

Equation 22 has the solution

$$X(n) = [c_2 \exp(k_r n) - c_1] / k_r \quad \dots(24)$$

where c_1 and c_2 , (constants for constant V and L), are to be determined from the boundary conditions pertaining at $n=1$ and N .

The M-tray stripping section may be treated similarly, (the reboiler being tray M), now modelling the equilibrium curve by the straight line

$$Y'(m) = \alpha_s X'(m) \quad \dots (25)$$

where $\alpha_s = 1/\alpha_r \quad \dots (26)$

for approximating a curve of constant relative volatility. This yields:

$$-k_s dX'(m)/dm = d^2X'(m)/dm^2 \quad \dots (27)$$

where $k_s = 2(V\alpha_s - L^*) / (V\alpha_s + L^*) \quad \dots (28)$

and $L^* = L + F \quad \dots (29)$

which has the solution:

$$X'(m) = [c_4 \exp(-k_s m) + c_3] / k_s \quad \dots (30)$$

The boundary conditions for the top and bottom of the rectifier and stripping section are respectively:

$$\left. \begin{aligned} VY(N-1) - VY(N) + LY(N) - LX(N) &= 0 \\ VY'(1) + LX(2) - VY(1) - LX(1) &= 0 \\ LX(1) + FZ + VY'(2) - VY'(1) - L^* X'(1) &= 0 \\ \text{and } L^* X'(M-1) - VY'(M) - (L^* - V)X'(M) &= 0 \end{aligned} \right\} \dots (31)$$

and substituting the solutions 24 and 30 into these boundary equations yield four independent equations for determination of the constants c_1 to c_4 . For example, taking $N = 29$, $M = 30$, $V = 25$, $F = 1$, $L = 24.5$, $Z = 0.5$, $\alpha_s = 1.04$ and $\alpha_r = 0.96$ yields numerical coefficients giving the solution:-

$$\begin{aligned} X(n) &= -48.5 [0.0147 \exp(-n/48.5) - 0.02474] \\ X'(m) &= 51.5 [0.0133 \exp(-m/51.5) - 0.003720] \end{aligned} \quad \dots (32)$$

giving terminal compositions $X(N) = 0.808$ and $X'(M) = 0.192$ which may be checked out by the McCabe-Thiel method. The important points to note are the similar values for c_2 and c_4 , $-k_r$ and k_s and that the spatial decrements $-1/k_r$ and $1/k_s$ are significantly larger than N and M permitting later simplifications. Another important point to stress here is that a mixture of low relative volatility, despite using many trays, can only be separated by employing reflux and V/F ratios much greater than those needed by mixtures of high α . The internal flows therefore greatly exceed the external flows.

3.2. High Frequency Dynamic Analysis

Linearising the dynamic version of equation 20 for the rectifying section for a plate holdup of H_r , and using the solutions derived in Section 3.1 for the quiescent operating conditions we obtain the following p.d.e. for $x(n,t)$

$$(\ell/L-v/V)(Lc_2/H_r)(1+k_r/2)\exp(k_r n) + a\partial x/\partial n + b\partial^2 x/\partial n^2 = \partial x/\partial t \quad \dots (33)$$

where $a = (L-V\alpha_r)/H_r \quad \dots (34)$ and $b = (L+V\alpha_r)/2H_r \quad \dots (35)$

It is required to obtain the frequency response between $x(n,t)$ and sinusoidal forcing functions $\ell(t) = \hat{\ell}\sin\omega t$ and $v(t) = \hat{v}\sin\omega t$. If we therefore set

$$f_1(t) = F_1 \sin \omega t \quad , \quad F_1 = \hat{\ell}/L-\hat{v}/V \quad \dots (36)$$

and spatial function

$$f_2(n) = (Lc_2/H_r)(1+k_r/2)\exp(k_r n) \quad \dots (37)$$

then we have

$$f_1(t)f_2(n) + a\partial x/\partial n + b\partial^2 x/\partial n^2 = \partial x/\partial t \quad \dots (38)$$

We approach the solution of (38) by breaking the spatial function $f_2(n)$ into a series of impulses, e.g. $f_2(n')\delta(n-n')$, equispaced at infinitesimal intervals dn' thus:

$$f_2(n) \equiv \sum_{n'=0}^N \delta(n-n')f_2(n')dn' \quad \dots (39)$$

and, having evaluated the response of p.d.e. 38 to one such impulse, summate the effects of all such impulses over the range $0 \leq n' \leq N$.

3.2.1. Response to Spatially-Concentrated Sinusoid

For this fictitious situation we have simply

$$a\partial x/\partial n + b\partial^2 x/\partial n^2 = \partial x/\partial t \quad , \quad n \neq n' \quad \dots (40)$$

Taylor's theorem cannot be applied across $n=n'$ however because of the point forcing function there present. We have instead, returning to the linearised dynamic mass balance equation at tray n' and reapplying Taylor's theorem:

$$f_1(t)f_2(n')\delta(n-n')dn' + (V\alpha_r/H_r)\left\{\partial x(n'-)/\partial n + 0.5\partial^2 x(n'-)/\partial n^2\right\} + (L/H_r)\left\{\partial x(n'+)/\partial n + 0.5\partial^2 x(n'+)/\partial n^2\right\} = \partial x(n')/\partial t \quad \dots (41)$$

(n'+) denoting n marginally >n' and (n'-) denoting n marginally <n'.

Now if $N \gg n', n \gg 0$... (42)

boundary conditions, at n=0 and N, may be neglected and the solution to p.d.e. 40 is then:

$$x(n,t) = c_n \exp\{-p(n-n')\} \sin\{\omega t - q(n-n') - \phi\} \quad \dots (43)$$

where the distance-dependent phase-shift and decrement have coefficients governed by

$$\left. \begin{aligned} p &= p_1, \quad q = q_1, \quad n > n' \\ p &= p_2, \quad q = q_2, \quad n < n' \\ q_1 &= -q_2 = \left[\{a^2 + (a^4 + 16b^2 \omega^2)^{0.5}\} / 8b^2 \right]^{0.5} \end{aligned} \right\} \quad \dots (44)$$

and $p_1 = \omega/2bq_1 + ab, \quad p_2 = \omega/2bq_2 + a/b$

The constants c_n , and ϕ may be determined by substitution of solution 43 and equations 44 in boundary condition 41 and, after tedious algebra, the following results emerge:

$$\phi = \tan^{-1}(2bq_1^2/\omega) \quad \dots (45)$$

$$c_n = 4F_1 f_2(n') \delta(n-n') dn' / b(4-a^2/b^2) \{ (p_1 - p_2)^2 + 4q_1^2 \} \quad \dots (46)$$

From solution 43 and the equations for constants p and q it is obvious that the response to the spatially concentrated input sinusoid shows an increasing phase-shift and attenuation with distance, $|n-n'|$, from the point of application of the input.

Figure 9 shows the response of liquid temperatures to a step-change in feedrate from a 12-tray pilot column separating a water-ethanol mixture at Sheffield. Because R was kept constant in this test, the disturbance resembles a true point disturbance at $m = M$ and the effect of the increasing attenuation and phase-shift with distance are clearly visible. The response differs fundamentally from that obtained with a distributed disturbance as will be demonstrated in Section 3.2.2. The decrement distance, $|1/p|$, is clearly frequency-dependent and the model is therefore only relevant for frequencies specified by

$$|1/p| \ll N/2 \quad \dots (47)$$

Now since $a/b \ll 1.0$, (equations 34 and 35), equations 44 simplify to give

$$p_1 = -p_2 \approx q_1 = -q_2 \approx (\omega/2b)^{0.5} \quad \dots (48)$$

and the condition for model validity, from 34, 47 and 48, is therefore:

$$\omega \gg 8b/N^2 \approx 8L/H_r N^2 \quad \dots(49)$$

For lower frequencies the terminal boundary conditions at $n=0$ and N must be considered.

3.2.2. Response to Spatially Distributed Forcing Function

Denoting the response to the concentrated input $f_1(t)f_2(n')\delta(n-n')dn'$ now as $\Delta_n x(n,t)$ we have from 3.2.1, and subject to 49,

$$\left. \begin{aligned} \Delta_n x(n,t) &= c_n \exp\{-p_1(n-n')\} \sin\{\omega t - q_1(n-n') - \phi\}, \quad n > n' \\ \text{and } \Delta_n x(n,t) &= c_n \exp\{-p_2(n-n')\} \sin\{\omega t - q_2(n-n') - \phi\}, \quad n < n' \end{aligned} \right\} \dots(50)$$

The response to the distributed input $f_1(t)f_2(n')$ will therefore be

$$x(n,t) = \sum_{n'=0}^N \Delta_n x(n,t) \approx \sum_{n'=-\infty}^{+\infty} \Delta_n x(n,t) \quad \dots(51)$$

$$\text{if } 0 \ll n \ll N \quad \dots(52)$$

as before.

Replacing the summation by integration and approximating $f_2(n')$, (equation 37), to

$$f_2(n') = (Lc_2/H_r)(1+0.25Nk_r) \quad \dots(53)$$

we obtain

$$x(n,t) = \frac{F_1(L/H_r)c_2(1+0.25Nk_r)}{\omega(1-0.25a^2/b^2)} \sin(\omega t - \phi - \beta) \quad \dots(54)$$

$$\text{where } \beta = \tan^{-1}(\omega/2bq_1^2) \quad \dots(55)$$

Unlike the case of point inputs, the response is now independent of distance, (provided $0 \ll n \ll N$), both in amplitude and phase since a comparison of equations 45 and 55 reveal that

$$\phi + \beta = \pi/2 \quad \dots(56)$$

This absence of lag between the response of consecutive trays to distributed inputs is verified by figure 10, which shows the effect of a step-change in vapour-rate on the Sheffield pilot-plant column. It was on such practical observations, here proved theoretically, that Stainthorp and Searson's

model³ was based, although they did allow for hydro-dynamic effects here neglected.

3.2.3. High-Frequency Transfer-Function Matrix

Results similar to equations 54 and 56 are obtainable for the stripping section. The transfer functions relating $x(n,t), x'(m,t)$ to $F_1 \sin \omega t$ are therefore both of an integrating nature at high-frequency due to the 90° phase-lags and the appearance of the single ω -term in the denominators. Combining these transfer-functions and rewriting F_1 in terms of \hat{v} and $\hat{\ell}$ (equation 36) yields a matrix equation relating the Laplace transformed variables, viz:

$$[\tilde{x}(m,s), \tilde{x}'(m,s)]^T = G(s) [\tilde{v}(s), \tilde{\ell}(s)]^T \quad \dots (57)$$

where

$$G(s) = \begin{bmatrix} c_2(1+0.25Nk_r)/s(1-0.25a^2/b^2)H_r V, & 0 \\ 0, & c_4(1-0.25Mk_s)\alpha_s/s(1-0.25\hat{a}^2/\hat{b}^2)H_s L^* \end{bmatrix} \begin{bmatrix} -L, & V \\ -L^*, & V \end{bmatrix} \quad \dots (58)$$

or, in terms of v and d ,

$$[\tilde{x}(n,s), \tilde{x}'(m,s)]^T = Q(s) [\tilde{v}(s), \tilde{d}(s)]^T \quad \dots (59)$$

where

$$Q(s) = \begin{bmatrix} c_2(1+0.25Nk_r)/s(1-0.25a^2/b^2)H_r V, & 0 \\ 0, & c_4(1-0.25Mk_s)\alpha_s/s(1-0.25\hat{a}^2/\hat{b}^2)H_s L^* \end{bmatrix} \begin{bmatrix} D, & -\bar{V} \\ -W, & -V \end{bmatrix} \quad \dots (60)$$

where $\hat{a} = (V\alpha_s - L^*)/H_s \quad \dots (61)$ and $\hat{b} = (V\alpha_s + L^*)/2H_s \quad \dots (62)$

3.3. Low Frequency Perturbations

Because of the boundary conditions, (which in 3.2 have been permissibly ignored for higher frequencies), a complete solution for a continuous infinite range of frequencies is very difficult to achieve. A geometrical approach based on the McCabe-Thiel diagram does however yield the behaviour of the system at perturbation frequencies sufficiently low to allow the dynamic terms in the process equations to be ignored. The high- and low-frequency models, if sufficiently similar in structure, may then hopefully be "joined together".

Figure 11 shows the diagram used for the geometrical analysis, but the angular deviations of the operating and equilibrium lines from the 45° line have been greatly exaggerated for reasons of clarity. The angle ϵ_r denotes the slope difference between these two lines in the rectifier and is given by

$$\epsilon_r = L/V - \alpha_r \quad \dots(63)$$

The angle γ between the equilibrium curve and the 45° line will be

$$\gamma = (1-\alpha_r)/(1+\alpha_r) \quad \dots(64)$$

If $\Delta Y(n)$ and $\Delta X(n)$ denote the vertical and horizontal distances between equilibrium and operating lines at tray n then a little consideration of the geometry reveals that

$$\Delta X(N) \approx \Delta Y(N) \approx \{1-X(N)\}2(1-\alpha_r)/(1+\alpha_r) \quad \dots(65)$$

and, furthermore,

$$\Delta X(n-1) \approx \Delta X(n) + 2\epsilon_r \Delta X(n) \quad \dots(66)$$

The total composition change, X_r , over the rectifier is therefore given by:

$$X_r = \sum_{i=1}^N \Delta X(N) [1+2\epsilon_r]^i \quad \dots(67)$$

and also

$$X_r \approx X(N) - Z \quad \dots(68)$$

Simplifying equation 67 by expanding as a power series in ϵ_r , neglecting all but the first order terms and replacing the summation by integration yields the equation:

$$2[1-X(N)]N(1+N\epsilon_r) \approx X(N)-Z \quad \dots(69)$$

the results from which agree closely with those derived from Section 3.1. We are here however interested in small perturbations from the steady-state and differentiating 69 with respect to forcing function ϵ_r yields the perturbation equation:

$$x(N) = 2(1-Z) \{N^2(1-\alpha_r^2)L/V [1+\alpha_r - 2(1-\alpha_r)N(1+N\epsilon_r)]^2\} \{L/V - v/V\} \quad \dots(70)$$

Noting that* $x(N/i) \approx x(N)/i \quad \dots(71)$

* $x(N/2)$ could be determined more precisely if necessary but we are here interested in trays in a generally central region.

and applying the same analysis to the stripping section yields the matrix equation

$$[x(n), x'(m)]^T = G_o [v, \ell]^T \quad \dots (72)$$

where

$$G_o = \begin{bmatrix} \frac{2(1-Z)Nn(1-\alpha_r^2)}{\{1+\alpha_r+2(1-\alpha_r)N(1+N\epsilon_r)\}^2 V^2} & , & 0 \\ 0 & , & \frac{2ZMm(\alpha_s^2-1)}{\{1+\alpha_s+2(\alpha_s-1)M(1+M\epsilon_s)\}^2 V^2} \end{bmatrix} \times \begin{bmatrix} -L & , & V \\ -L^* & , & V \end{bmatrix} \quad \dots (73)$$

or, in terms of v and d,

$$[x(n), x'(m)]^T = Q_o [v, d]^T \quad \dots (74)$$

where

$$Q_o = \begin{bmatrix} \frac{2(1-Z)Nn(1-\alpha_r^2)}{\{1+\alpha_r+2(1-\alpha_r)N(1+N\epsilon_r)\}^2 V^2} & , & 0 \\ 0 & , & \frac{2ZMm(\alpha_s^2-1)}{\{1+\alpha_s+2(\alpha_s-1)M(1+M\epsilon_s)\}^2 V^2} \end{bmatrix} \times \begin{bmatrix} D & , & -V \\ -W & , & -V \end{bmatrix} \quad \dots (75)$$

Now merely by inspection of the high and low frequency transfer-function matrices G, Q, and G_o, Q_o structural similarities are immediately obvious and an overall transfer-function matrix equation of the form, say,

$$\begin{bmatrix} x(n, s) \\ x'(m, s) \end{bmatrix} = \begin{bmatrix} k_1/(1+T_1 s) & , & 0 \\ 0 & , & k_2/(1+T_2 s) \end{bmatrix} \begin{bmatrix} D & , & -V \\ -W & , & -V \end{bmatrix} \begin{bmatrix} \tilde{v}(s) \\ \tilde{d}(s) \end{bmatrix} \quad \dots (76)$$

would appear to fit both frequency domains. k₁, k₂, T₁ and T₂ are directly calculable from the appropriate elements of Q and Q_o which in turn are directly calculable from the basic plant parameters and via the constant-defining equations given in the paper.

Substituting parameter values, the 59-tray column of Section 3.1 is found to have the full-frequency-range transfer function matrix: (for $n=m=15$),

$$Q(s) = \begin{bmatrix} 17.10^{-4}/(1+3.4H_r s) & 0 \\ 0 & 16.6.10^{-4}/(1+3.58H_s s) \end{bmatrix} \begin{bmatrix} 0.5 & -25.0 \\ -0.5 & -25.0 \end{bmatrix} \dots (77)$$

which may clearly be diagonalised by application of merely a static pre-compensator $Q(o)^{-1}$. Unlike the short column of section 2 no simple pairing of input and output variables would yield acceptable interaction. This is basically due to the large V/F ratio required to separate mixtures of low relative volatility.

The long column model, (equation 76), is found to give useful predictions for columns of only moderate length. A 20-tray column, (N=9, M=11), for instance, separating a mixture of $\alpha=1.39$, (equivalent to $\alpha_s \approx 1.25$, $\alpha_r \approx 0.80$), is found to have the transfer-function matrix: (for $n=m=5$),

$$Q(s) = \begin{bmatrix} 0.0890/(1+6.05H_r s) & 0 \\ 0 & 0.180/(1+12.70H_s s) \end{bmatrix} \begin{bmatrix} 0.5 & -2.0 \\ -0.5 & -2.0 \end{bmatrix} \dots (78)$$

, (when operating at $V = 2.5$, $L = 2.0$, $Z = 0.5$, $F = 1.0$), and this claim is verified by figure 11 which shows a comparison between the computed step-responses of the non-linear process with that of the linearised transfer-function model, for a step in V from 2.0 to 3.0 at $D = 0.5$. The agreement is remarkable in view of the very large step in V, the comparative shortness of the column, and the severe non linearities of the simulated process arising from the use of the true equilibrium curve and the multiplicative nature of the inputs.

4. Discussion and Conclusions

Original analytical transfer function models have been developed for both very small and very long columns. Like the small column, the multi-tray column's transfer-function exhibit 90° of phase-shift at high frequency suggesting that a matrix of simple time constants would describe any column. This observation is consistent with the models of other authors such as Stainthorp³, McMoran⁷ and Osborne et al¹¹. It must be remembered however that the long column model has been derived for trays in the central regions of the rectifier and stripping sections, (which is appropriate to conventional feedback control techniques in

practice), but the boundary conditions imposed by highly mismatched accumulator and reboiler vessels could conceivably cause greater phase-shifts over the intermediate frequency range $0 < \omega < 8L/H_r N^2, 8L^*/H_s M^2$ in columns of intermediate length yielding the travelling-wave effects sometimes apparently observed in practice⁴ though rarely, except in Pigford's work¹² produced by computer or reduced-order models. Whether or not such phenomena if revealed, by virtue of their low frequency, have a significant bearing on the performance of a control system is uncertain and merits further investigation.

Much simulation has however validated the model here proposed for a wide range of column sizes and, on the basis of such a model, it is concluded that, whereas any simple pairing of input and output variables fails to eliminate interaction as columns become longer, a simple, non-dynamic precompensator is all that is required to eliminate not only inter-loop detuning but also interaction of a transient nature. This is possible as a result of the very simple dynamic structure of the process which allows all interaction problems to be investigated merely from a knowledge of static characteristics. It is concluded also that the detuning effects of multiple loop closure are predictable, for columns at least, by an inverse Nyquist method considerably simpler than the computer based inverse Nyquist array technique of Rosenbrock¹⁰ and with far greater certainty.

Finally it should be noted that the columns and separations examined have been of a fairly symmetrical physically. However it is believed that the approaches outlined here could be extended fairly simply to cover non-symmetric equilibrium curves and rectifiers and stripping sections of unequal size. A badly sited feed tray would cause difficulty however because of the uneven spatial distribution of composition which this would cause so prohibiting the linearising of this distribution in the analysis (equation 53).

5. Acknowledgements

The authors are grateful for the encouragement given in their research in process modelling by Professor H. Nicholson, Head of the Department of Control Engineering at Sheffield, and for his making available the computing and pilot plant facilities in support of this work. The use of the U.M.I.S.T. inverse-Nyquist array C.A.D. package, via the Sheffield-U.M.I.S.T. link, is also gratefully acknowledged.

6. References

1. Wilkinson, W.L. and Armstrong, W.D.: Chemical Eng. Science, 1957, Vol.7, No.1/2, pp.1-7.
2. Wood, R.M. and Armstrong, W.D.: *ibid*, 1960, Vol.12, pp.272-276.
3. Stainthorp, F.P. and Searson, H.M.: Trans. Instn. Chem. Engrs., 1973, Vol.51, pp.42-55.
4. Shinsky, F.G.: 'Process control systems', McGraw-Hill, New York, 1967, 367pp.
5. Davison, E.J.: Trans. Instn. Chem. Engrs., 1967, Vol.45, p.229.
6. Chan, A.L. and Talbot, F.D.: Canadian Journal of Chemical Engg., 1975, Vol.53, pp.91-95.
7. McMorran, P.D.: Proc. of 4th U.K.A.C. Control Convention, 1971, p.122.
8. Judson King, C.: 'Separation processes', McGraw-Hill, New York, 1971, 809pp.
9. Rosenbrock, H.H.: Report by rapporteur, I.Chem.E. Symposium Series, 1969, No.32, p.6:4.
10. Rosenbrock, H.H.: 'Computer-aided control system design', Academic Press, London, 1974, 230pp.
11. Osborne, Jr., W.G., Reynolds, D., West, J.B. and Maddex, R.N.: A.I.Ch.E.-I.Chem.E. Symposium Series, 1965, No.1, p.84.
12. Lamb, D.E., Pigford, R.L. and Rippin, D.W.T.: Chem.Eng.Prog., Symposium Series No.36, 1961, Vol.57, pp.132-147.

7. Symbols Used

- | | | |
|----------------------|---|--|
| α | = | Relative volatility of binary mixture |
| α_r, α_s | = | Mean slopes of equilibrium curves in rectifier and stripping sections in the long column, and their point values in the short column |
| a, a' | = | Coefficients of 1st spatial derivative of composition w.r.t. plate no. in p.d.e.'s describing rectifier and stripping section |
| b, b' | = | Coefficients of 2nd spatial derivative of composition w.r.t. plate no. in p.d.e.'s |
| β | = | Phase-shift angle |
| c_1, \dots, c_4 | = | Constants in steady-state composition distribution equations |
| γ | = | Angle between equilibrium line and 45° line of McCabe-Thiel diagram |
| D, d | = | Distillate molar flow rate and small perturbation therein |

δ	= Unit impulse function
ϵ_r, ϵ_s	= Difference in slope between equilibrium and operating lines on McCabe-Thiel diagram
$\Delta X(n), \Delta Y(n)$	= Horizontal and vertical distances between equilibrium and operating lines of McCabe-Thiel diagram at tray n
F	= Molar flow rate of feed stream
$f_1(t), F_1$	= Sinusoidal time-varying component of column forcing function and its peak value
$f_2(n)$	= Spatial distribution of column forcing function
G, g_{11}, \dots, g_{22}	= Transfer-function matrix relating mid column compositions to \tilde{v} and \tilde{d} and elements thereof
H, h_{11}, \dots, h_{12}	= General 2x2 transfer-function matrix and elements thereof
H_r, H_s	= Molar holdups of each theoretical tray in rectifier and stripping section
k_r, k_s	= Constants relating to spatial decrements of steady-state composition distributions
k_1, k_2	= Gain terms of final transfer-function model
L, ℓ	= Reflux molar flow and small perturbation therein
L^*	= Liquid molar flow in stripping section
m, M	= General tray number in stripping section and its maximum value
n, N	= General tray number in rectifier and its maximum value
P_1, P_2	= Frequency-dependent constants relating to spatial decrements of sinusoidal composition perturbations
q_1, q_2	= Frequency-dependent coefficients relating to phase shift of sinusoidal composition perturbations
Q, q_{11}, \dots, q_{12}	= Transfer function matrix relating mid column compositions to \tilde{v} and \tilde{d} and elements thereof
ϕ	= Phase-shift angle
R	= Reflux ratio, (L/D)
s	= Laplace operator w.r.t. time, t
S	= Separation
T_r, T_s	= Time constants of rectifier and stripping sections (short column)
T_1, T_2	= Time constants of entire rectifier and stripping sections (long column)
V, v	= Molar vapour flow rate and small perturbation therein

- W = Molar flow rate of bottom product
- X,x = Mol fraction of light component in liquid in rectifier,
and small perturbation therein
- X',x' = Mol fraction of light component in liquid in stripping
section, and small perturbation therein
- Y,y = Mol fraction of light component in vapour in rectifier,
and small perturbation therein
- Y,y' = Mol fraction of light component in vapour in stripping
section, and small perturbation therein
- Z = Mol fraction of light component in feed stream
- ω = Angular frequency of sinusoidal perturbations
- \tilde{v}, \dots denotes Laplace transform of v w.r.t. time, etc.
- Superscript T denotes the Transpose of a matrix
- Suffix o denotes steady-state model

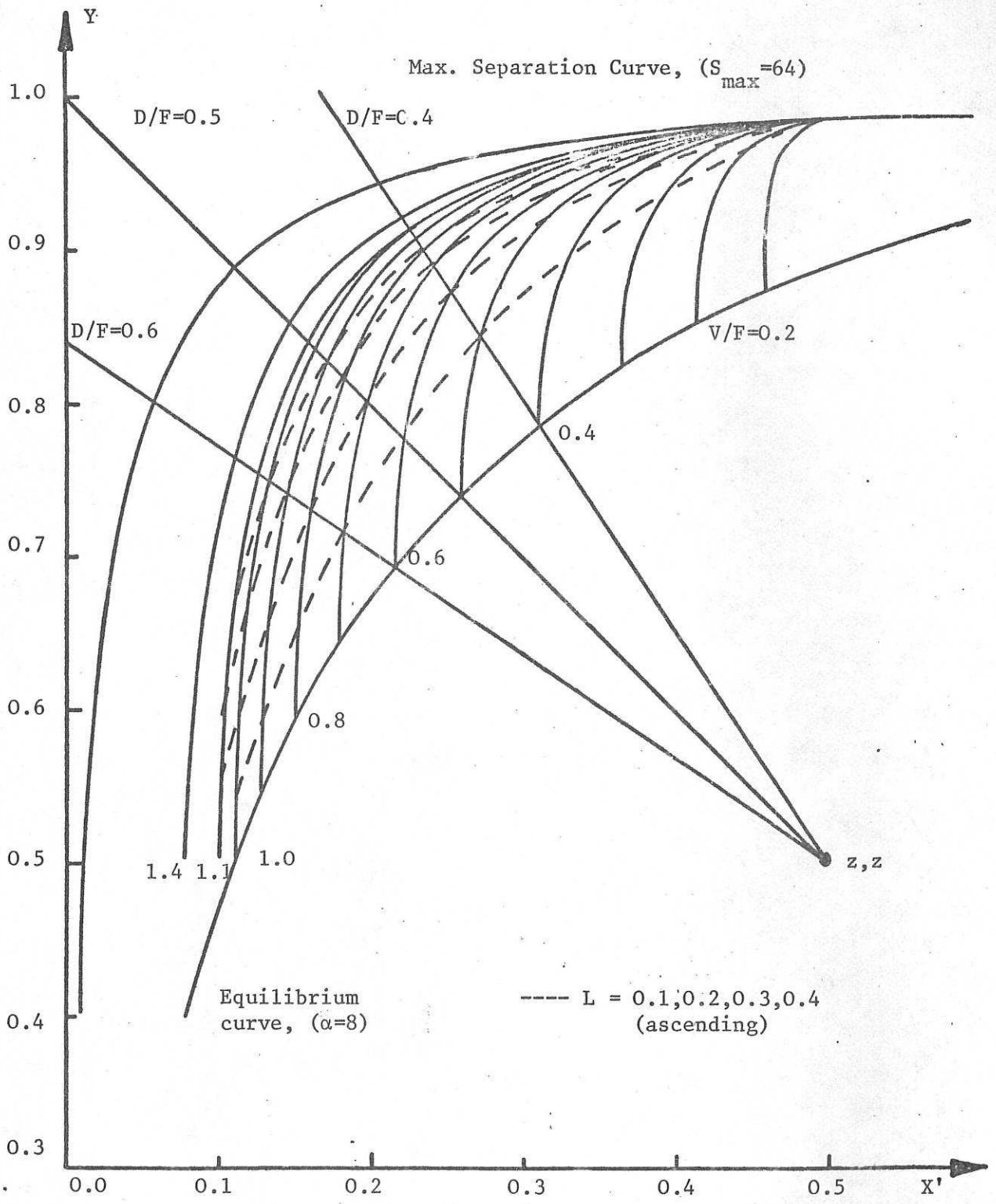


Fig. 1. Single-tray Rectifier Column: Steady-State Characteristics

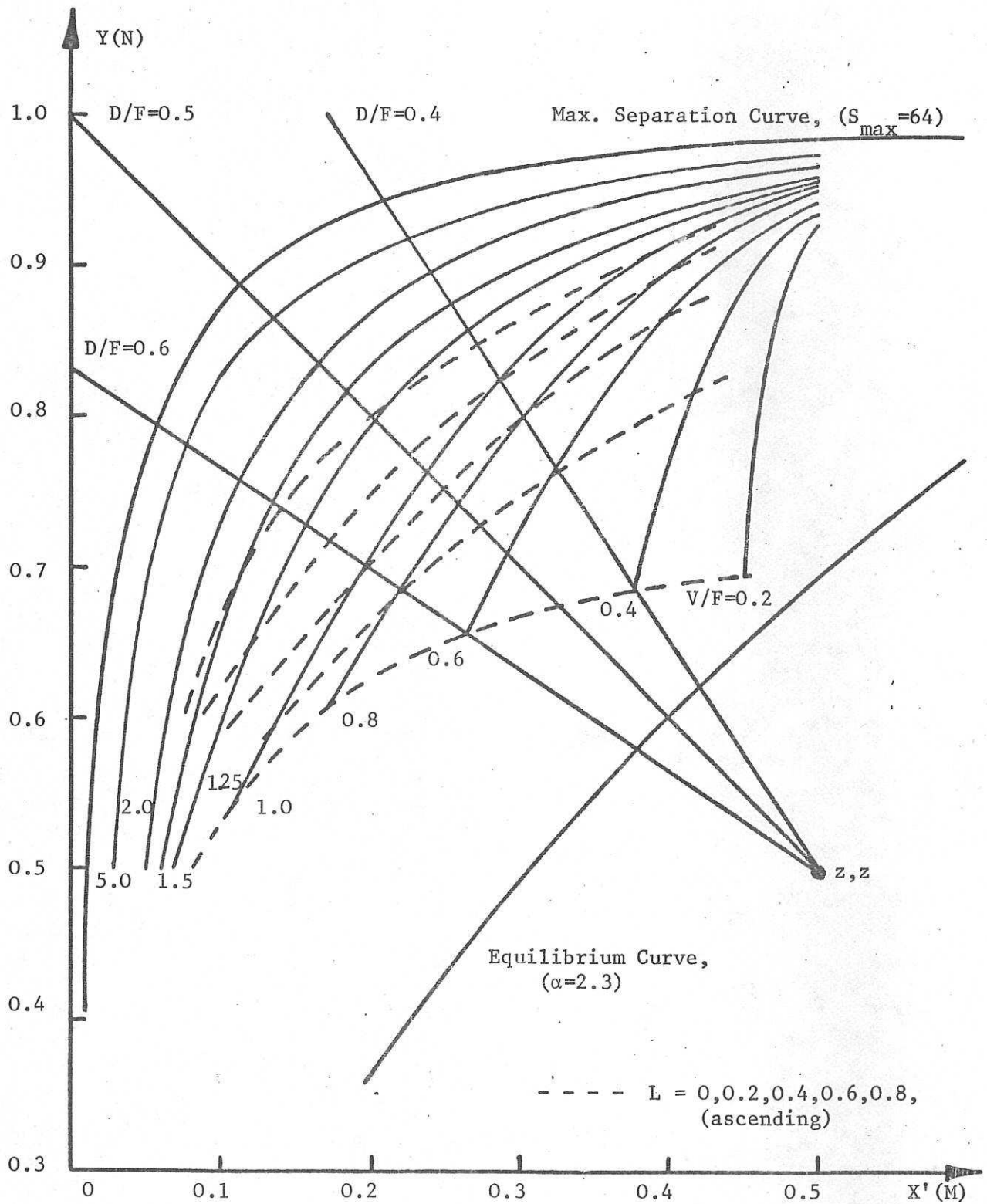


Fig. 2. Four-tray Column: Steady-State Characteristics

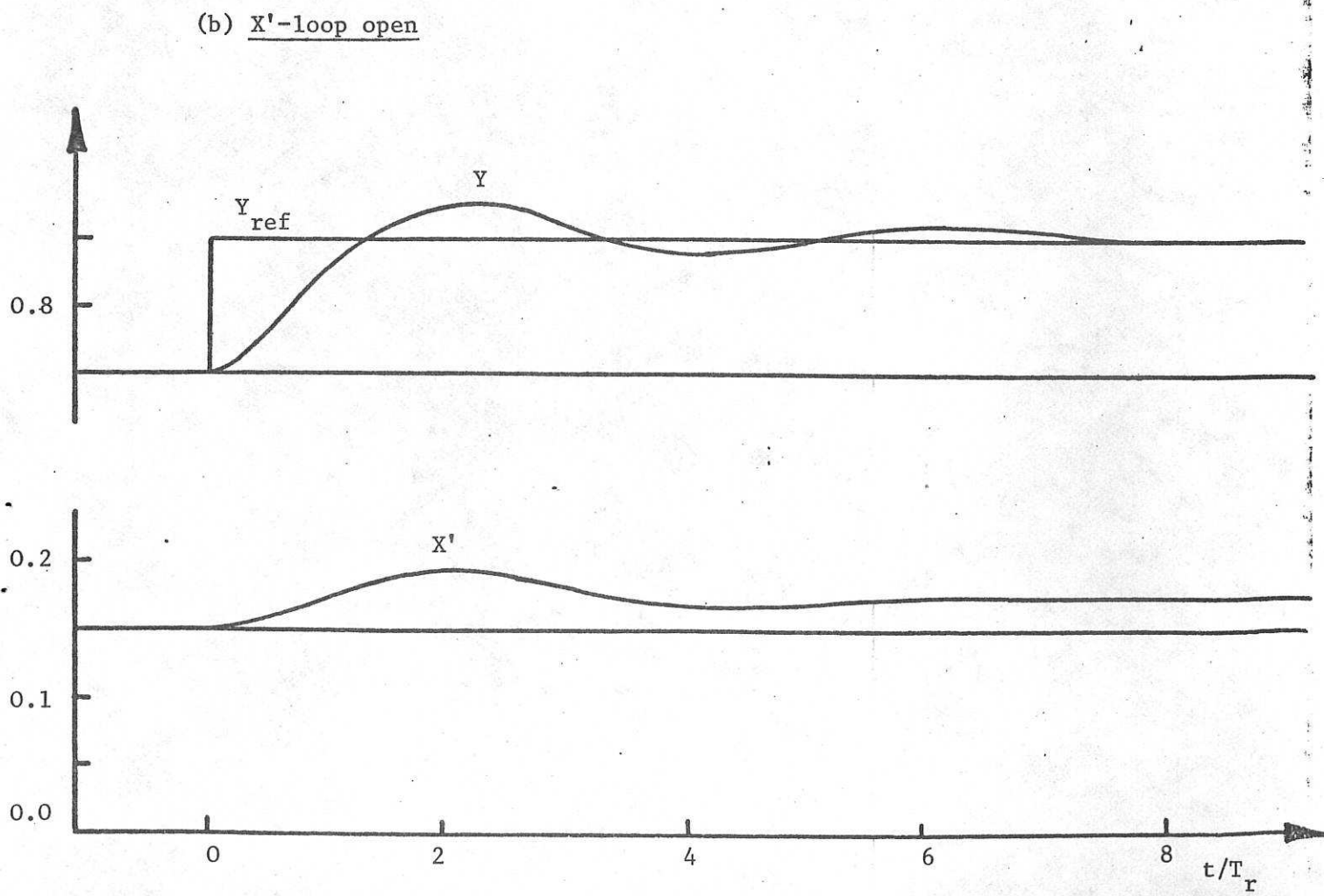
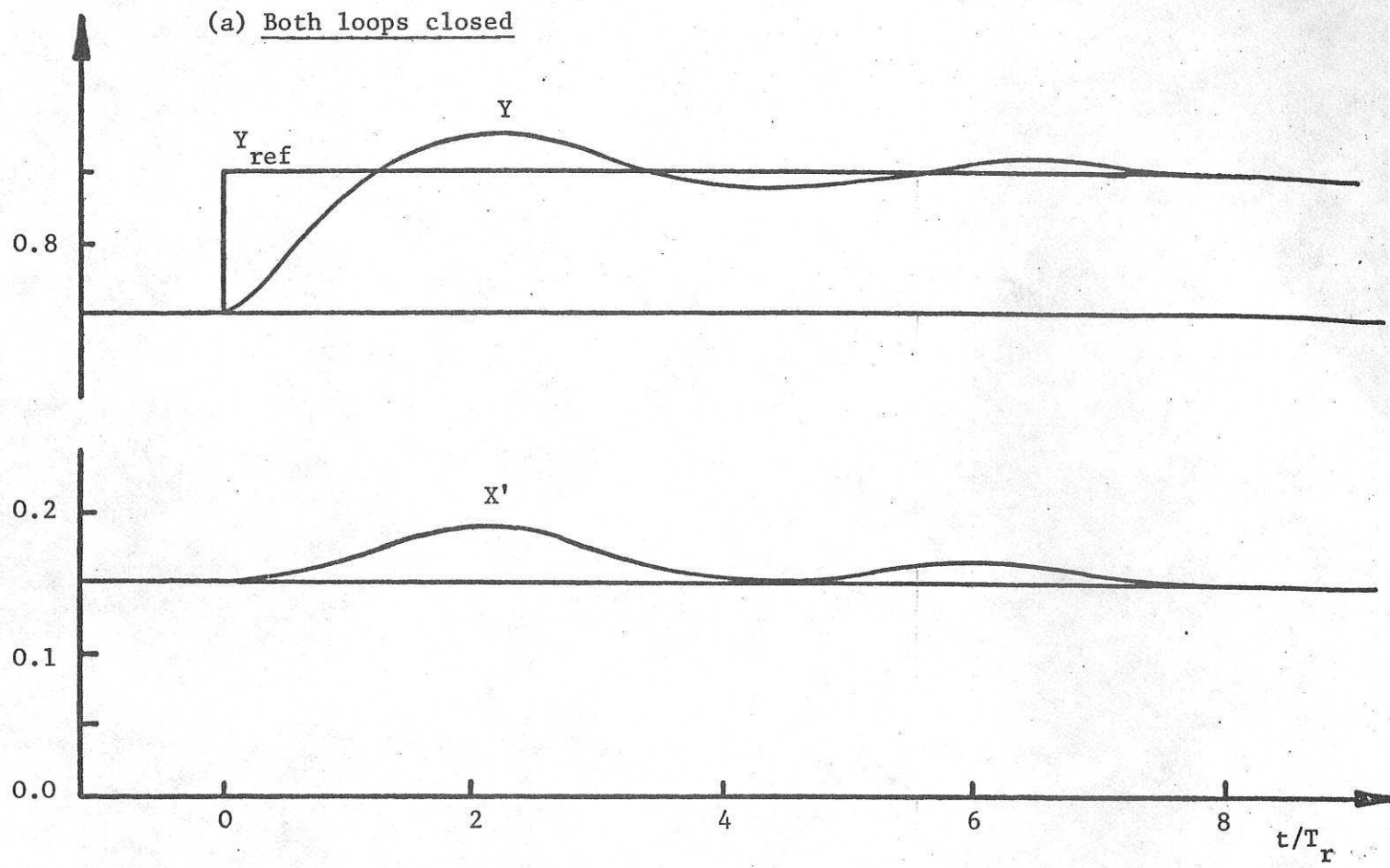


Fig. 3. Showing interaction effects between control-loops when Y sets D/F and X' sets V/F

(a) Both loops closed
(b) X'-loop open

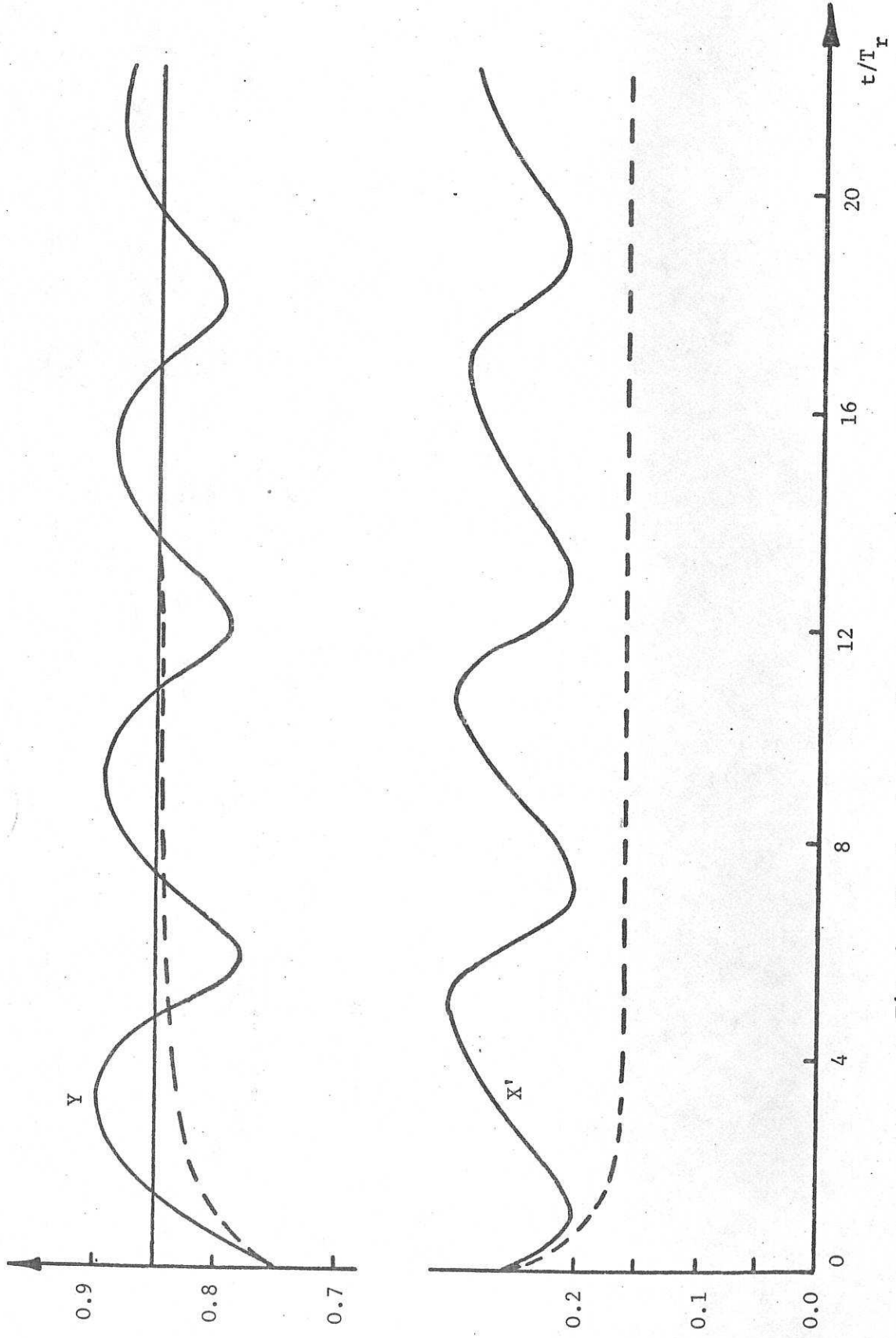


Fig. 4. Showing interaction effects between control loops when Y sets V/F and X' sets D/F

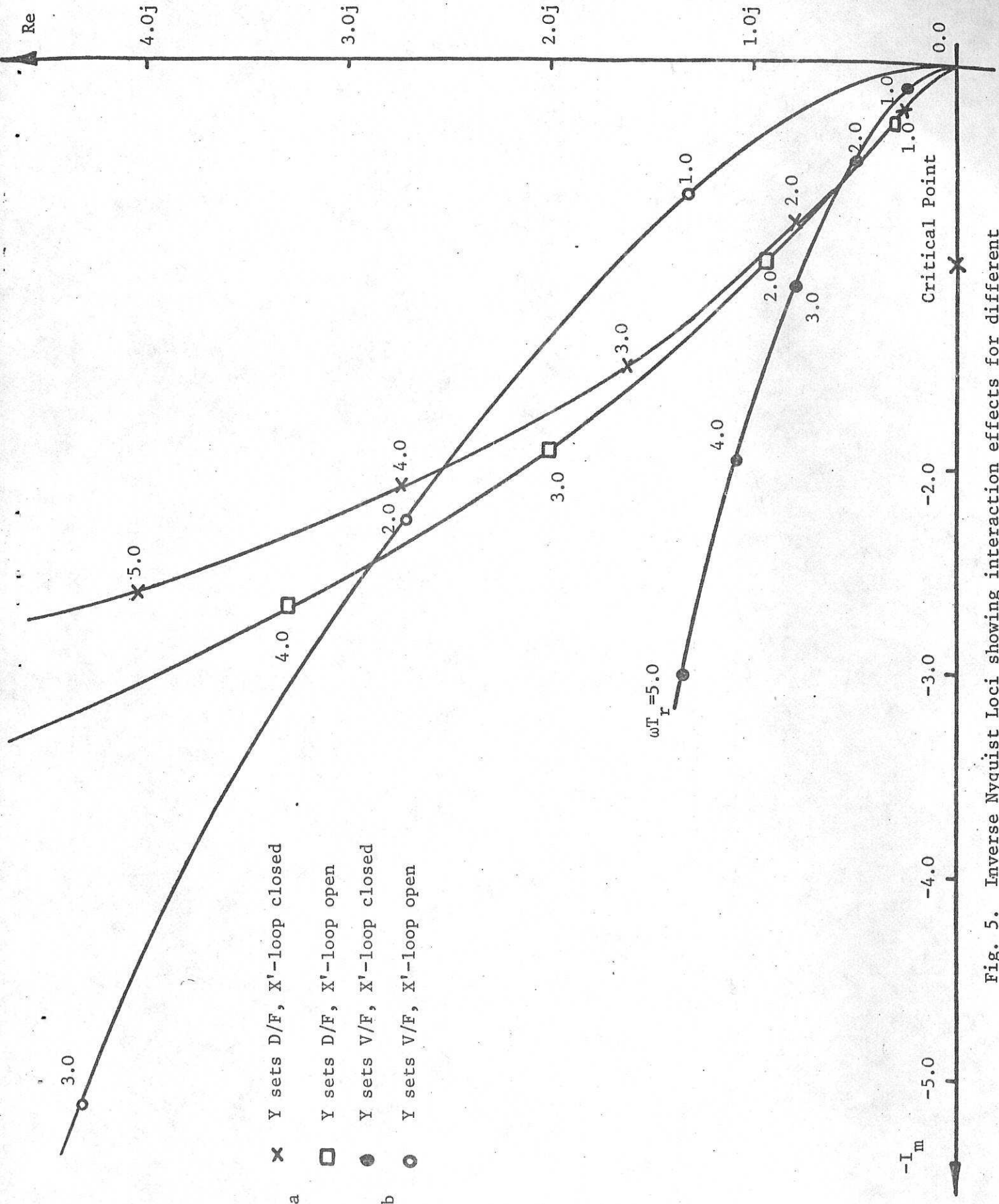


Fig. 5. Inverse Nyquist Loci showing interaction effects for different couplings of Y and X' with V/F and D/F

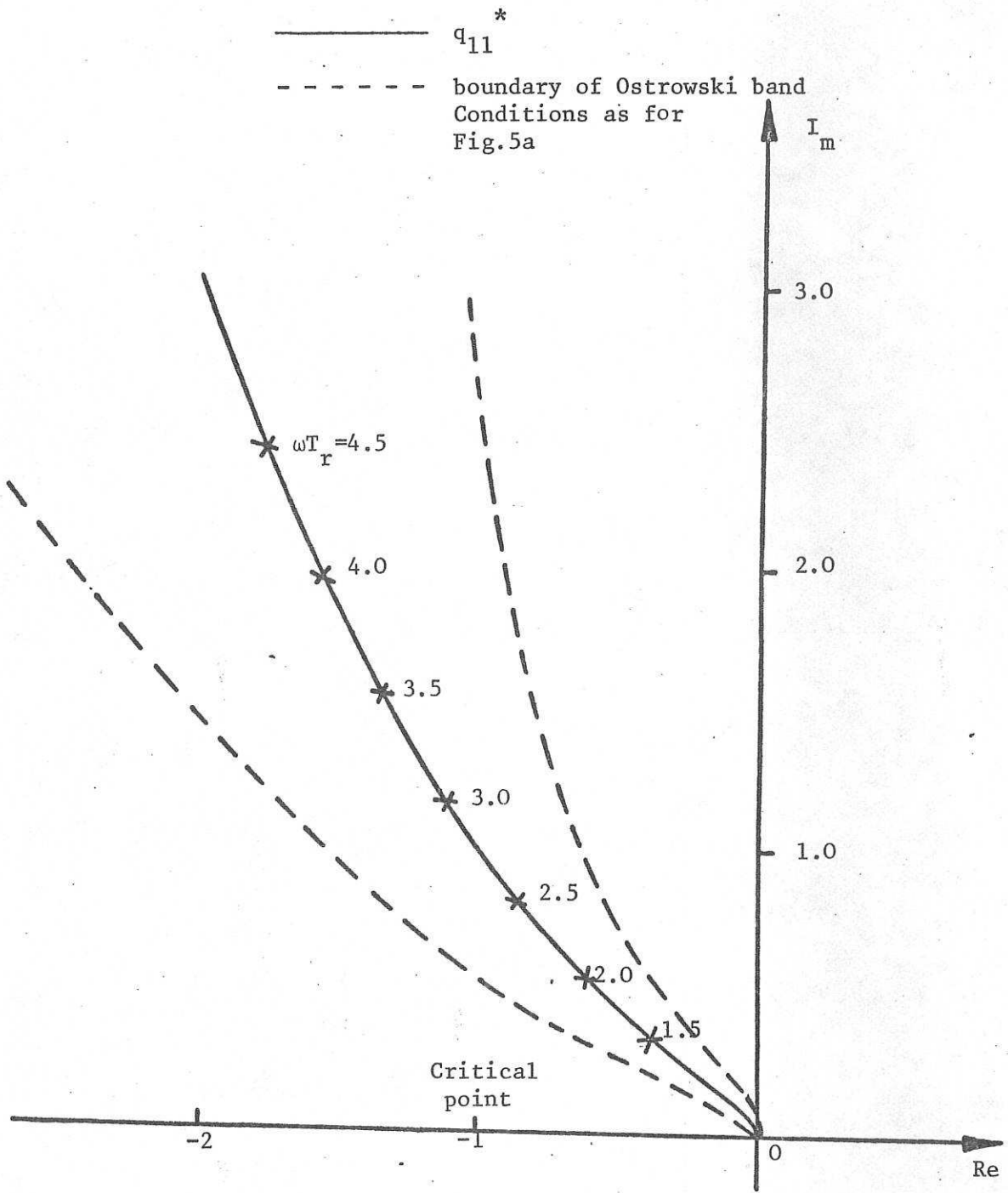


Fig. 6. Inverse Nyquist Array element h_{11}^* with boundary of Ostrowski circles

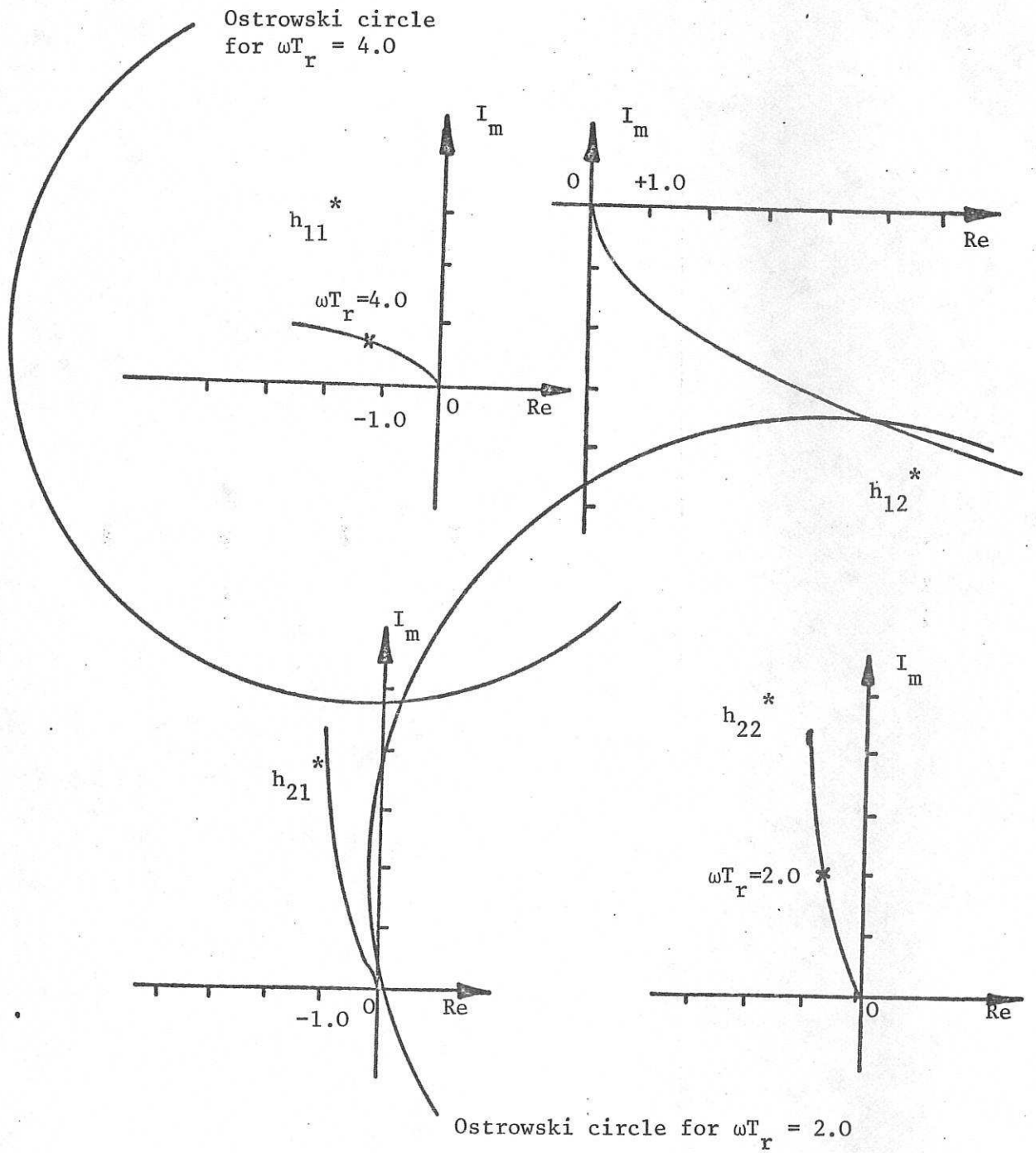


Fig. 7. Inverse Nyquist Array H^*

----- boundary of Ostrowski bands

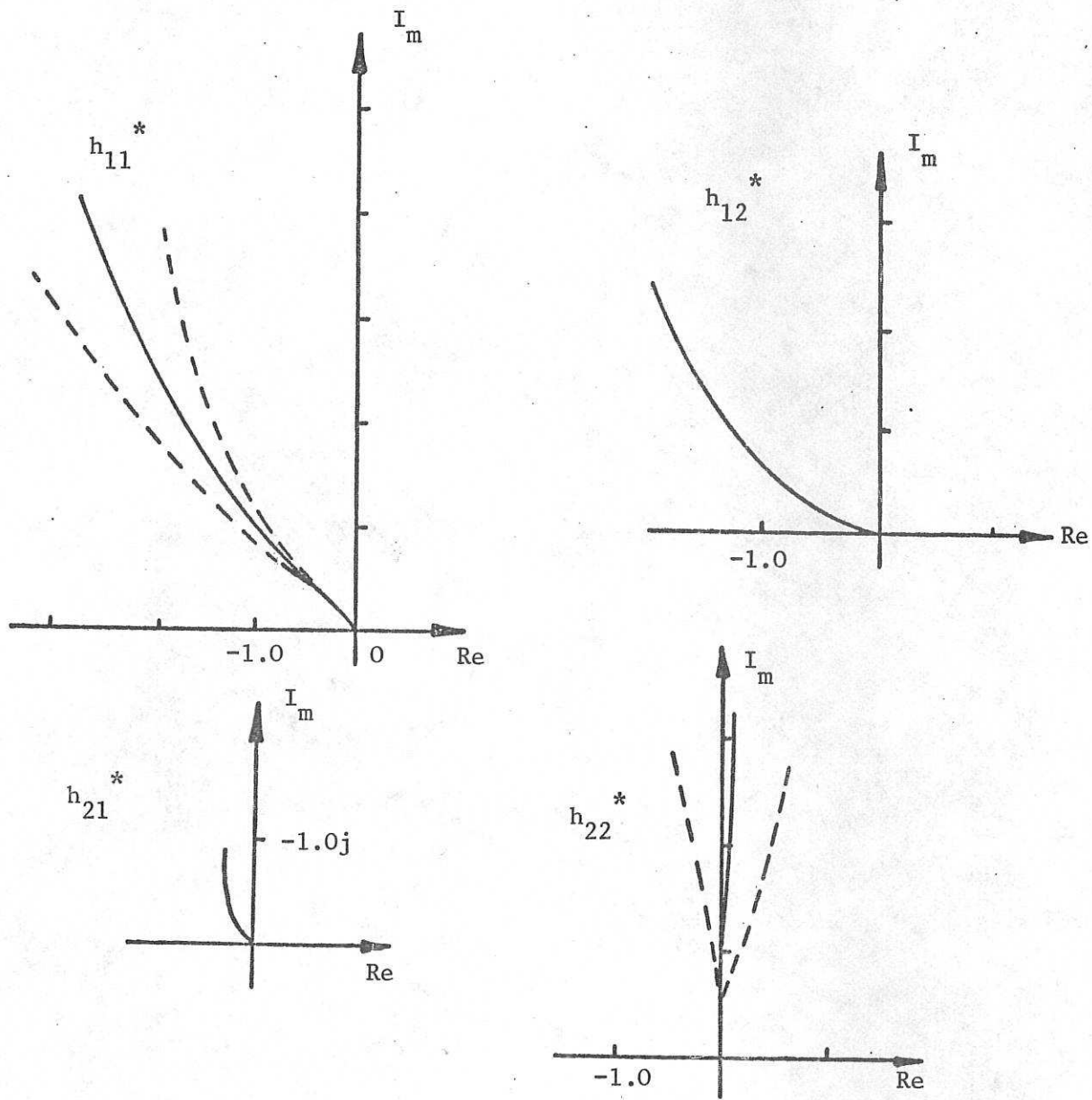
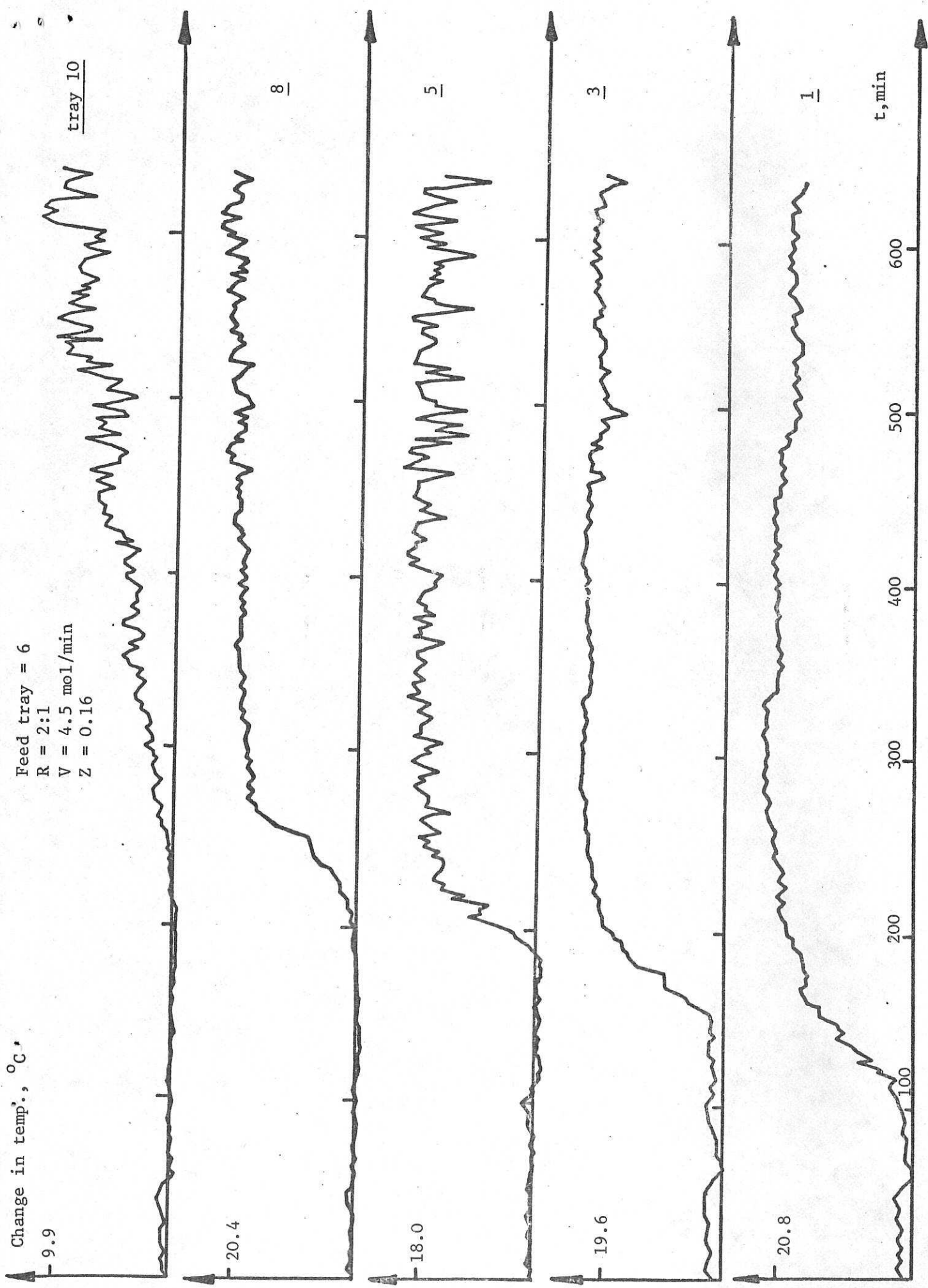


Fig. 8. Inverse Nyquist Array for Process with precompensator $G^{-1}(o)$



Feed tray = 6
 R = 2:1
 V = 4.5 mol/min
 Z = 0.16

Fig. 9. Temperature response of 12-tray, water/ethanol pilot column to decrease in F from 8.8 to 6.3 mol/min (at 96 min)

Change in temperature, °C

Feed tray = 6

R = 2;1

F = 8.8 mol/min

Z = 0.16

tray 10

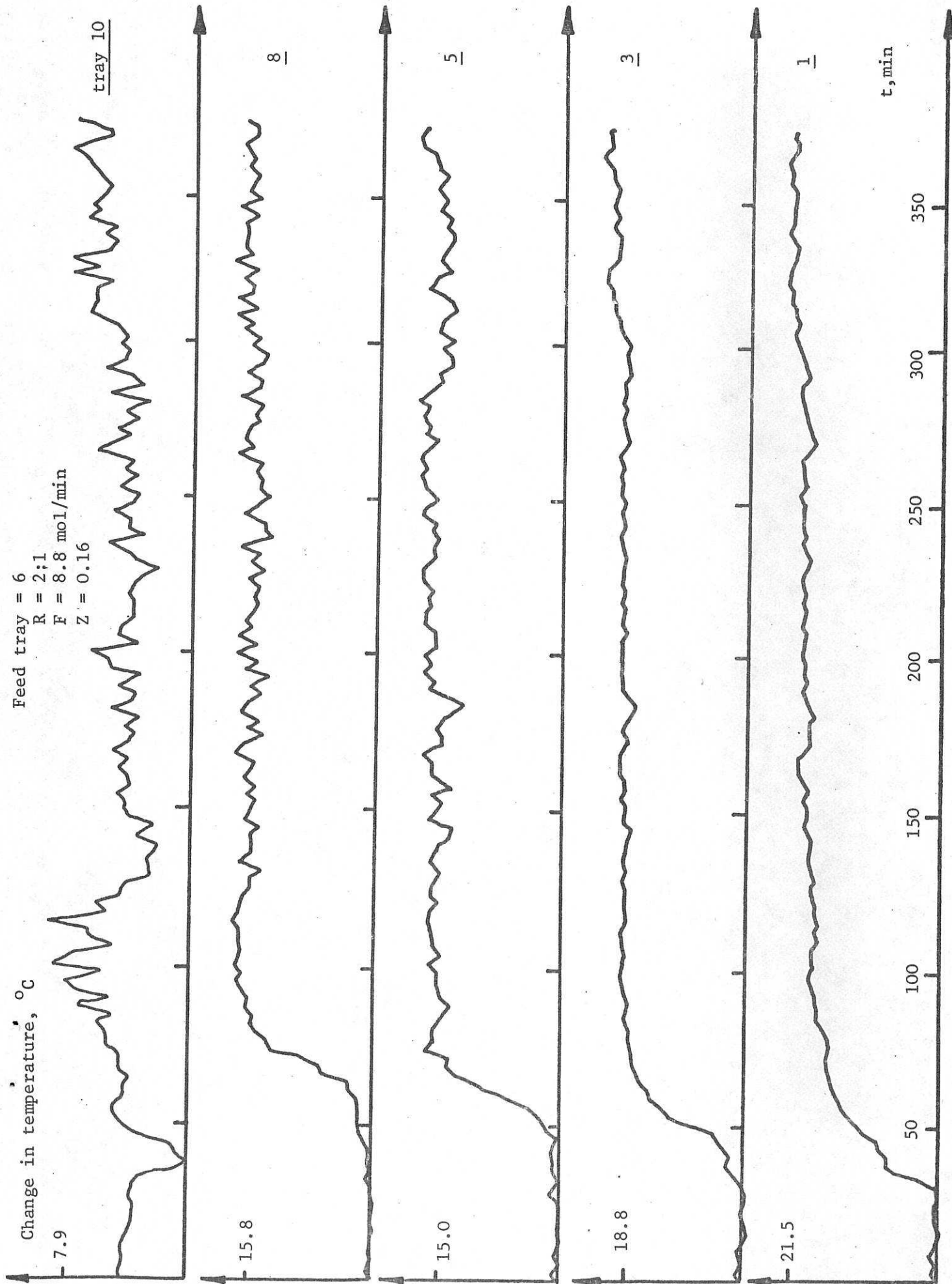


Fig. 10. Temperature response of 12-tray, water/ethanol pilot column to increase in V from 5.0 to 8.0 mol/min (at 26 min)

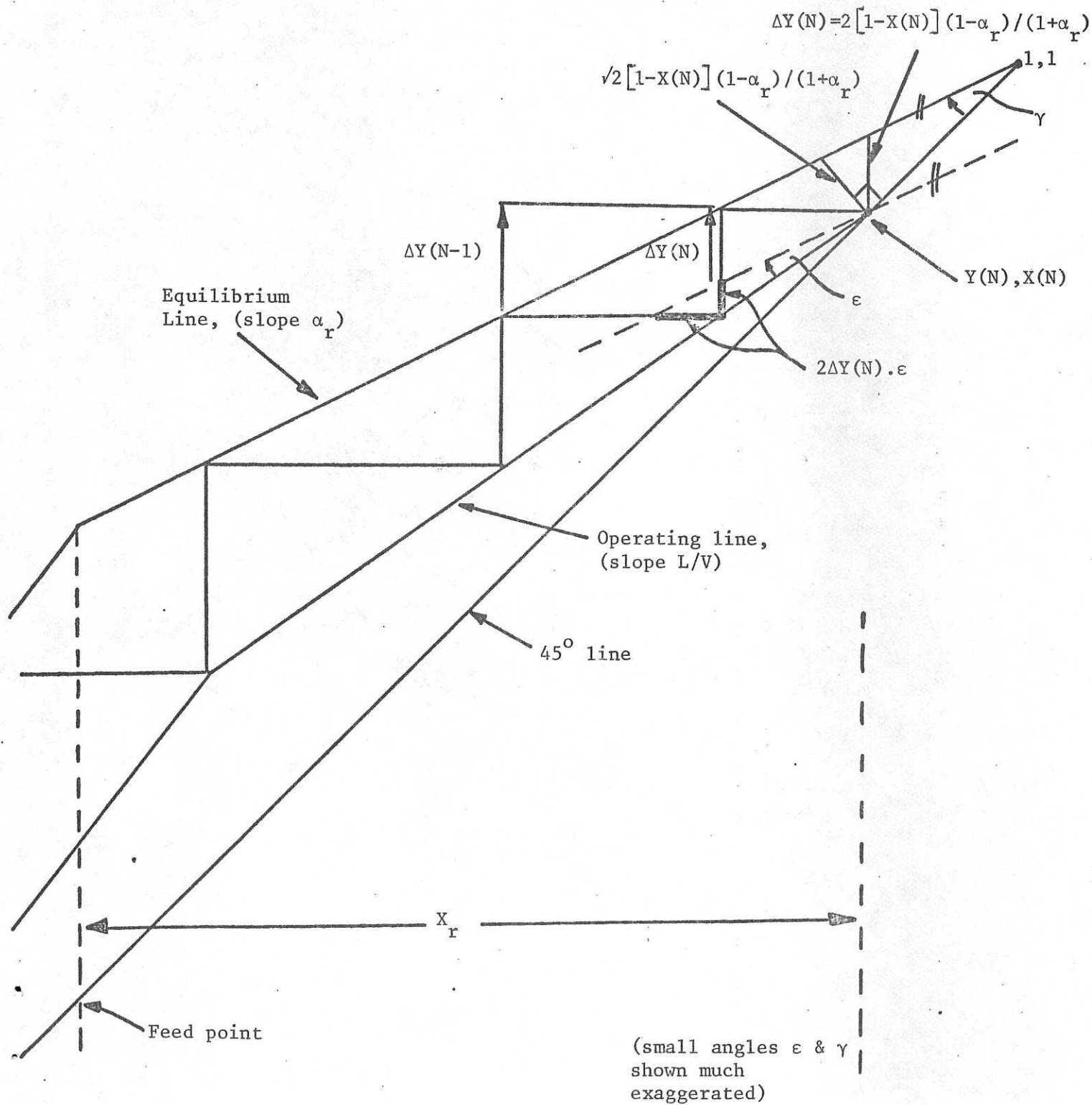


Fig. 11. McCabe-Thiel diagram for determination of constant perturbations

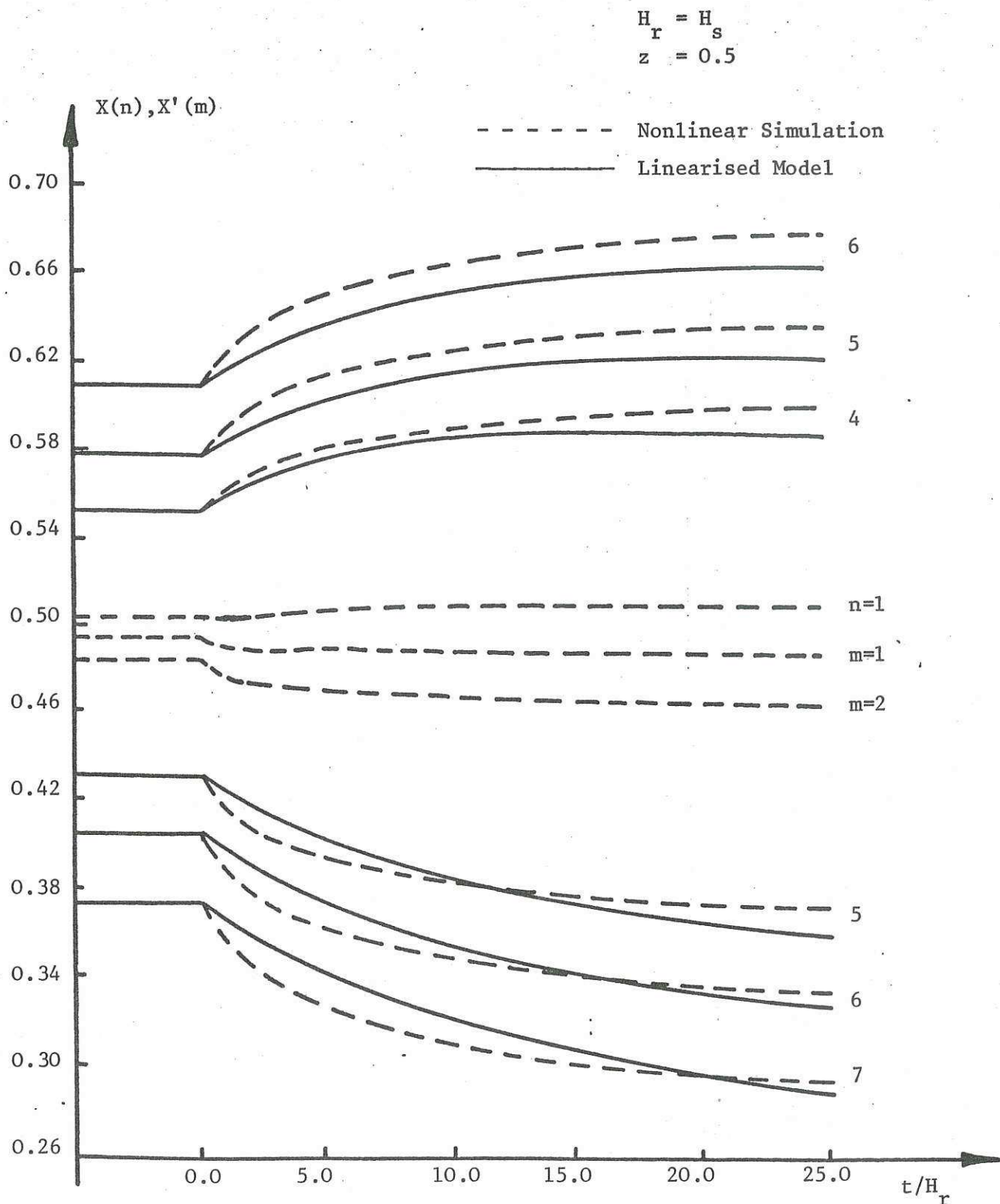


Fig. 12. Response of 20-tray column to increase in V/F from 2.0 to 3.0